RSC Advances

PAPER

View Article Online
View Journal | View Issue

Cite this: *RSC Adv.*, 2015, **5**, 24864

A polymerized ionic liquid functionalized cathode catalyst support for a proton exchange membrane CO_2 conversion cell†

P. Tamilarasan and S. Ramaprabhu*

This study aims at the efficient conversion of CO_2 to formic acid using a proton exchange membrane cell by selective functionalization of a cathode catalyst support. We chose polymerized ionic liquid (PIL) as the surface functional moiety, since CO_2 has good solubility in it. A multiwalled carbon nanotube (MWNTs) surface was functionalized with PIL and used as a cathode catalyst support. This novel catalyst support shows extremely good affinity towards CO_2 and facilitates better dispersion of catalyst nanoparticles. Catalytic nanoparticles were decorated over the catalyst supports by a microwave assisted polyol reduction method, which gives better dispersion of finer particles on PIL functionalized MWNTs compared to pure MWNTs. The protonation of CO_2 to formic acid has been studied in a polymer electrolyte membrane (PEM) CO_2 conversion cell with synthesized catalysts. The cells were tested under continuous and discontinuous CO_2 supply, where PIL functionalized MWNTs show a better formic acid formation rate than the pure support under identical experimental conditions, due to the improved interaction between the catalyst support and CO_2 molecules.

Received 16th February 2015
Accepted 2nd March 2015

DOI: 10.1039/c5ra03002a

www.rsc.org/advances

1. Introduction

Valorization of carbon dioxide by catalytic, photocatalytic and electrocatalytic processes has attained importance, since it provides a vital route to achieve the twin goals of reducing atmospheric CO_2 levels and obtaining valuable chemical feedstocks to promote energy storage.[1–3] Formic acid is one of the main products from CO_2 protonation, which has been identified as a promising liquid feed for fuel cells with moderate specific hydrogen density (43.5 g of H_2 per kilogram), energy density (1700 W h kg^{-1}) and low-toxicity.

The advantage of polymer electrolyte membranes (PEM) is well recognized in fuel cells. The reverse action of fuel cell can be employed for protonation of CO_2 to fuels, which has an advantage in prevention of products from re-oxidation. Several studies on PEM cell based electrochemical conversion of CO_2 into useful hydrocarbons have been reported.[4,5] Delacourt *et al.* have fabricated and evaluated various configurations of PEM CO_2 conversion cells.[6] In addition, the product distribution is narrow and can be tuned by the altering the surface chemistry and applied potential in potentiostatic mode. The continuous electrochemical conversion of CO_2 into formate using PEM cell has been reported, where lead or tin plates were used as cathode, individually.[7,8] Narayanan *et al.*, has reported a PEM cell based electrochemical system with alkaline and alkali ion transport membrane, for carbon dioxide conversion into formates.[5]

The technological advantages of supported nanoparticles have been well realized in electrochemical applications.[9,10] Catalyst supports have been chosen based on their surface area, anchoring sites and electrical conductivity and their favorability in the specified catalytic reaction. Multiwalled carbon nanotubes (MWNTs) provide an improved nanoscale 3D architecture due to their randomly entangled 1D structure, which allows a better three-phase contact between electrode, electrolyte and reactant.[11] In addition, the honeycomb lattice allows wide variety of covalent or non-covalent surface functionalization and to tune the local surface chemistry.[12]

According to the rate law of chemical reaction, the local CO_2 concentration is one of the factors governing the conversion rate. Inclusion of functional moieties on MWNTs surface is a possible way to improve local CO_2 concentration without increasing gas pressure.[13,14] It is reported that CO_2 has good solubility in imidazolium based ionic liquids (IL).[15,16] In addition, CO_2 forms a weak complex with imidazolium cations through the nitrogen sites.[17] This suggests a good and reversible interaction between imidazolium based ionic liquid and CO_2 molecules. It is also observed a strong correlation between the local surface chemistry of electrode and the overpotential necessary to drive the reduction. Ionic liquid cation forms weak complex with the charged

Alternative Energy and Nanotechnology Laboratory (AENL), Nano Functional Materials Technology Centre (NFMTC), Department of Physics, Indian Institute of Technology Madras, Chennai, 600036, India. E-mail: ramp@iitm.ac.in

† Electronic supplementary information (ESI) available. See DOI: 10.1039/c5ra03002a

intermediate and stabilizes them, which leads to a positive shift in the reduction potential.[17]

It is reported that the polymerized ionic liquids (PIL) have even higher CO_2 sorption capacity along with faster sorption/desorption rates than monomers.[18,19] Recently, we have studied the influence of IL or PIL functionalization on CO_2 adsorption properties of graphene, which shows that PIL functionalization improves the CO_2 adsorption capacity and energy.[20,21] Based on this property, we could demonstrate the higher CO_2 conversion rate with PIL functionalized catalyst supports in our recent study.[22] Here, PIL functionalization improves the localized CO_2 (reactant) concentration, which reduces the hydrogen generation. Thus, the rate of CO_2 electro-reduction is increased by effective utilization of produced protons.[17] Recently, Aeshala *et al.*, have observed improved hydrogenation of CO_2 along with 50% less H_2 generation, if the anchoring functional groups are introduced at the three phase boundary.[23]

Generally, H_2 dissociation ability of noble metal catalysts (Pt, Ru and Rh) have been well realized in PEM fuel cells and PEM water splitting cell, which can be used for CO_2 protonation as well. Although Pt has low HCOOH formation efficiency, we chose it in order to highlight the advantage of PIL functionalization.[24] Moreover, Pt shows the high effective barrier (1.56 eV) for formic acid dehydrogenation compared with Pd (0.76 eV) and Ni (1.03 eV), which may prevent the produced formic acid from catalytic dissociation.[25]

In this report, we have demonstrated the potential advantages of surface functionalization of cathode catalyst support (MWNTs) with PIL moieties in CO_2 conversion applications. Here, we take advantage of the benefits that CO_2 is highly soluble in ionic liquid and PIL functionalized MWNTs as catalyst support to develop a novel, task-specific catalyst support for CO_2 conversion. To the best of our knowledge, this is the first report on PIL functionalized MWNTs as catalyst support for CO_2 conversion applications.

2. Experimental section

2.1 Material synthesis

Platinum nanoparticle decorated PIL surface functionalized MWNTs was synthesized by a three step route (see ESI 1† for brief description). In the first step, MWNTs were synthesized by catalytic chemical vapor deposition and purified by air oxidation and acid treatment.[26] MWNTs surfaces were functionalized with PIL by free radical polymerization of [VMIM][BF_4] in second step.[27] Finally, decoration of Pt nanoparticles (20 wt%) over the surface of MWNTs and MWNTs–PIL was carried out by microwave assisted polyol reduction method.[27]

2.2 Materials characterization

Molecular vibrational analysis of synthesized materials was carried out by Perkin-Elmer Fourier transform infrared (FTIR) spectrometer. Structural analyses were carried out by X'Pert Pro PANalytical powder X-ray diffractometer and the data are analyzed by X'Pert High Score Plus package. The surface morphology of was carried out using field emission scanning electron microscopy (FESEM) and high-resolution transmission electron microscopy (HRTEM) using FEI Quanta and Technai G-20, respectively. Low-pressure CO_2 adsorption isotherms were determined by a surface area analyzer (Micromeritics ASAP 2020) at 298 K sample temperature for various pressures up to 100 kPa. Carbon dioxide conversion analysis has been carried out by PEM cell, which mimics a conventional fuel cell. The CO_2 conversion rate, by means of concentration of formic acid, was determined by a calibrated Perkin-Elmer spectrophotometer.

3. Results and discussions

3.1 Morphological analysis

The electron microscope images of MWNTs (Fig. 1(a & d)) show tubular nature of 1D carbon nanotubes with smooth surface. In

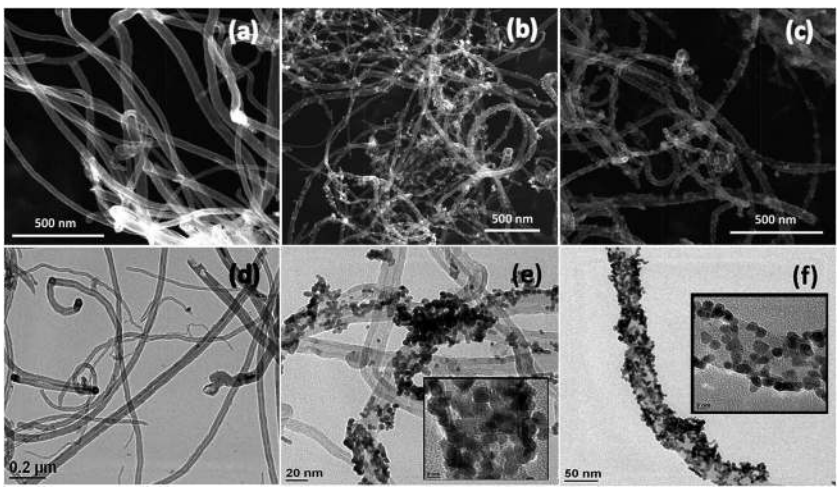

Fig. 1 FESEM images of (a) MWNTs, (b) Pt/MWNTs, (c) Pt/MWNTs–PIL and TEM images of (d) MWNTs, (e) Pt/MWNTs and (f) Pt/MWNTs–PIL (insets: respective high magnification images).

addition, the absence of amorphous carbon and catalyst impurities clearly suggests purity.

We found a great degree of agglomeration of Pt nanoparticles on the surface of MWNTs (Fig. 1(b)) due to the rapid reduction of metal ions by microwave. Purified MWNTs has fewer amounts of surface anchoring sites, such as functional groups and structural defects. Since the density of anchoring and nucleation sites is less, the particles are nucleated at very few sites and results in bigger particle size. Moreover, the grown particles may not be anchored with enough energy, which leads to a great degree of agglomeration. It is observed that the particles are highly distributed over MWNTs–PIL support compared to pure MWNTs. The PIL functionalization offers a uniform distribution of surface anchoring/nucleation sites, which leads to a better dispersion of fine nanoparticles. The inset in Fig. 1(f) clearly displays that the particle size is less than 5 nm along with highly uniform distribution.

3.2 Structural analysis

The X-ray diffractogram (Fig. 2) of MWNTs reveals the peak at 26.3° corresponding to the (002) plane of MWNTs. Decoration of Pt nanoparticles introduces diffraction patterns corresponding to Pt at 40.1°, 46.7°, 68° and 81.9° with both MWNTs and MWNTs–PIL support. It is worth to note that the peaks corresponding to Pt are more broadened in the case of MWNTs–PIL support. The crystal size of Pt nanoparticles is calculated from the peak centred at 40.1° using Scherrer formula and found to be 5.3, 2.9 nm for MWNTs, MWNTs–PIL catalyst supports, respectively. This is a strong evidence for the better particle anchoring ability of PIL functionalized support and is in good agreement with literature.[28]

3.3 Molecular vibrational analysis

The molecular vibrational characterization of MWNTs, MWNTs–PIL and Pt/MWNTs–PIL has been carried out by Fourier Transform Infrared (FTIR) analysis in order to confirm PIL moieties. FTIR spectra of MWNTs–PIL and Pt/MWNTs–PIL are shown in Fig. 3. The band corresponding to stretching vibrations (~3450 cm^{-1}) and in-plane bending (~1405 cm^{-1}) vibrations of

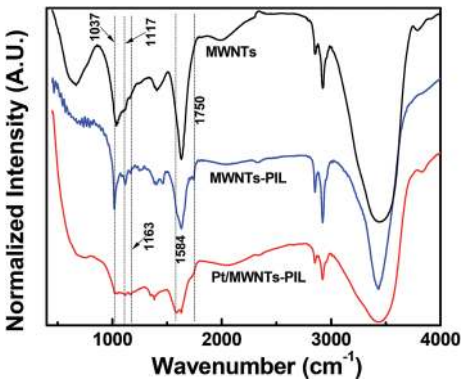

Fig. 3 FTIR spectrum of MWNTs, MWNTs–PIL and Pt/MWNTs–PIL.

hydroxyl/carboxyl group occur due to the presence of moisture and surface hydroxyl functionalities. The stretching vibration of aromatic rings (hexagonal honeycomb lattice) has been found at ~1636 cm^{-1} in all samples, while the ring-breathing mode is identified at 1037 cm^{-1}. The peaks at fingerprint region (500–1500 cm^{-1}) can be assigned to the various stretching and bending modes of residual functional groups on MWNTs.[29] Briefly, the stretching mode of C–O–H (1117 cm^{-1}), vibrations of ketone (1163 cm^{-1}) and other possible C/H/O compounds (broad peak 550–850 cm^{-1}) can be confirmed.

The relative intensities of anti-symmetric and symmetric $=CH_2$ vibrations at 2922 and 2853 cm^{-1} of MWNTs–PIL is quite prominent than that of MWNTs. This may be attributed to the presence of PIL on the surface of MWNTs. Moreover, C=N stretching (1750 cm^{-1}) and imidazolium ring stretching vibrations (1584 cm^{-1}) have born upon PIL functionalization. It is notable that the peaks corresponding to PIL appears even after Pt decoration. This confirms that PIL moieties are unaffected even after strong microwave irradiation and repeated washing.[30]

3.4 Carbon dioxide adsorption studies

Carbon dioxide adsorption properties of MWNTs and MWNTs–PIL (Fig. 4) were determined at 283 K sample

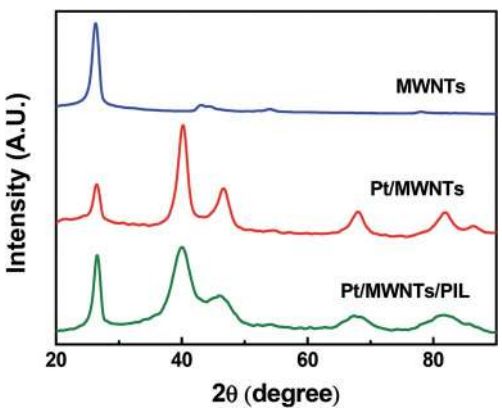

Fig. 2 X-ray diffractogram of MWNTs, Pt–MWNTs and Pt/MWNTs–PIL.

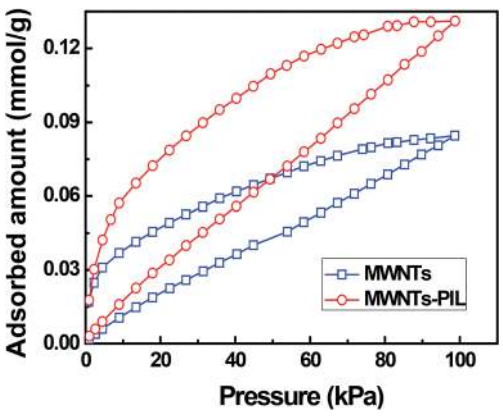

Fig. 4 Carbon dioxide adsorption properties of MWNTs and MWNTs–PIL at 283 K.

temperature for various pressures up to 100 kPa in order to know the affinity towards CO_2 molecules using surface area analyzer. Polymerized ionic liquid functionalized MWNTs show ~55% higher CO_2 capturing capacity than that of MWNTs due to the better CO_2–PIL interaction, which is a direct proof for the advantage of PIL functionalization in this application. This is in good agreement with our previous report.[31] Moreover, desorption curve also shows that MWNTs–PIL retains higher percentage of CO_2 at lower equilibrium pressures, which suggests that MWNTs–PIL can hold relatively higher amount of CO_2 even at low partial pressures.

3.5 Electrochemical analysis (half cell measurement)

The electrochemical activity of prepared catalysts has been determined by cyclic voltammetry, using a typical three-electrode system in 1 M H_2SO_4 solutions, where platinum wire and saturated Ag/AgCl electrodes were used as counter and reference electrode, respectively.

A typical working electrode was prepared by drop casting catalyst on glassy carbon electrode. Briefly, 1 mg of catalyst was dispersed in 0.25 ml of 0.5 wt% Nafion + isopropanol solution by ultrasonication. The slurry, containing 20 μg (52 μg cm^{-2} Pt loading) catalysts, was drop casted on glassy carbon electrode (0.076 cm^2). The cyclic voltammetry was experimented at 50 mV s^{-1} scan rate (Fig. 5). The electrochemical oxidation peak in the forward scan, located between −0.2 to 0.2 V (inset in Fig. 5) can be assigned to hydrogen desorption from Pt surfaces, which clearly suggests that PIL functionalization improves the electrochemically active surface area. This can be attributed to the high physical/electrochemical surface area of Pt nanoparticles due to the reduced particle size as suggested by X-ray diffraction pattern.

The electrocatalytic reduction behaviour of CO_2 on Pt/MWNTs and Pt/MWNTs–PIL electrode with CO_2 saturated 0.5 M $KHCO_3$ was evaluated by half cell measurement using cyclic voltammetry (Fig. 6) at 50 mV s^{-1} scan rate. Here, the glassy carbon electrode was modified with the electrocatalyst and used as a working electrode in three electrode measurement system. We observed the reduction signals at −0.62 and −0.48 V with respect to standard hydrogen electrode (SHE) for Pt/MWNTs,

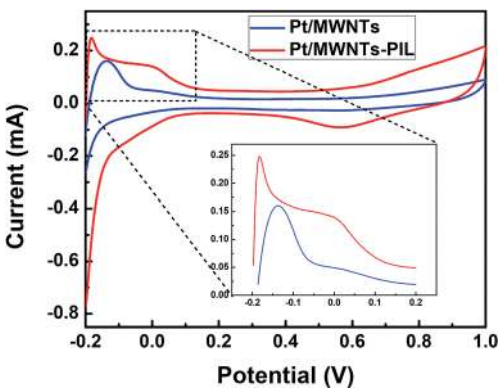

Fig. 5 Cyclic voltammogram of Pt/MWNTs and Pt/MWNTs–PIL electrode. Electrolyte: 1 M H_2SO_4, reference electrode: saturated Ag/AgCl electrode.

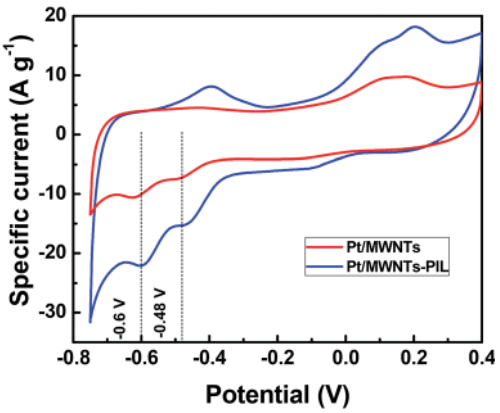

Fig. 6 Cyclic voltammogram of CO_2 reduction on Pt/MWNTs and Pt/MWNTs–PIL electrode. Electrolyte: CO_2 saturated 0.5 M $KHCO_3$, reference electrode: saturated Ag/AgCl electrode.

which can be assigned to the formation of HCOOH and HCHO, respectively, in good agreement with the existing literature.[24,32] Similar reduction potentials were reported by Lu *et al.*, for Pd–MWNTs system.[33] Moreover, the peak current is significantly improved upon PIL functionalization due to the accumulation of CO_2 at the conversion site, as we observed in our previous study.[22]

It has to be noted that Pt/MWNTs–PIL shows a slight positive shift in reduction peak at −0.6 V, which may be attributed to the local PIL moieties. Haan *et al.* have reported that the reduction potential of CO_2 on platinum surface shifts positively in ionic liquids medium.[34] Here, IL moieties stabilize the charged intermediates and shifts the potential of rate-limiting step to more positive potentials.[17,35]

In addition, we observed a peak around −0.4 V in the forward scan, which is strengthened upon PIL functionalization. This may be assigned to the electrosorption of reduced CO_2 (*CO_2 radical) on catalyst.[36] However, it needs further investigation to confirm the claim. It is also important to note that the double layer contribution with Pt/MWNTs–PIL is slightly higher than Pt/MWNTs. The surface roughness of the catalyst support is increased upon PIL functionalization, which leads to higher ion (K^+ or H^+) adsorption through double layer formation. It has to be pointed out here that the mass transfer behaviour will be different in half-cell and full-cell measurements. Here, electrons, protons and CO_2 are readily available for reaction. But in full-cell measurement, electrons and protons must be produces from water at anode and transported to cathode. This leads to additional potential for electroreduction of CO_2 into formic acid.

Conclusively, the improvement may be attributed to three major reasons:

(1) The better dispersion of Pt nanoparticles, which increases the physical/electrochemical surface area of Pt and thus the activity.

(2) The high affinity of PIL functionalities towards CO_2, which increases the amount of CO_2 in contact with the electrocatalyst and significantly increases conversion rate.

(3) The formation of charged intermediates or complexes with adsorbed CO_2 at the ionic liquid (particularly with imidazolium) sites during the rate-determining step may assist the effective reduction of carbon dioxide.

3.6 CO_2 conversion analysis (full cell measurement)

Pt/MWNTs and Pt/MWNTs–PIL were used as cathode material in PEM CO_2 conversion cell fabrication without further modification. The structure of PEM CO_2 conversion cell mimics typical PEM water electrolysis cells used for hydrogen production (see Fig. S1†). Here, Pt loading was maintained to be 0.5 and 1 mg cm^{-2} at anode and cathode, respectively, for all the experiments. Since liquids can closely reach the catalyst, we used high purity CO_2 dissolved in DI water (33 mM at 298 K temperature and 1 bar CO_2 equilibrium pressure) as a source of carbon dioxide. Deionized water was used as base fluid, since pH of CO_2 saturated water is 5–6 that favours the interaction of CO_2 and its intermediates with Pt surface.[37] The detailed fabrication and analysis procedure have been given in ESI 2.†

In a typical experiment, a positive potential was applied to the anode with respect to cathode. The cathode reservoir solution was sampled after 90 min and analyzed by FTIR spectroscopy, in order to confirm the formation of hydrocarbon molecule (Fig. 7). The traditional stretching and bending vibrations of –OH group occur in all samples at around 3300 cm^{-1} and ~1650 cm^{-1}, respectively, from the base fluid. The asymmetric stretching vibrations of CO_2 molecule occurs at 2345 cm^{-1} in the spectra of CO_2 saturated deionized water. In addition, the weak signals of symmetric and asymmetric stretching vibrations of C–H group are also found at 2926 and 2853 cm^{-1}, due to the trace amount of carbonic acid generally present in carbonated water. The stretching vibrations of C–H group are strengthened upon hydrogenation of CO_2, which confirms the formation of hydrocarbon. Moreover, the signal corresponding to molecular CO_2 (~2330 cm^{-1}) has been weakened after 30 min of reaction, since CO_2 is converted into hydrocarbon.[29] Thus the conversion product was confirmed to be a hydrocarbon.

Further, the cathode reservoir solution samples were analyzed by UV-Vis spectrophotometer in order to determine the hydrocarbon molecule. The optical spectrum shows a peak with maxima between 230–240 nm, which matches well with commercial formic acid and is in good agreement with literature (Fig. 8).[5,22] Hence, spectrophotometer was calibrated using commercial formic acid by serial dilution method and employed for quantitative analysis of formic acid production, where CO_2 saturated deionized water was used as reference. The optical absorption spectra were fitted to Gaussian function after baseline correction and the peak height was considered for formic acid concentration determination.

The electrochemical analysis reveals that the CO_2 hydrogenation potential is −0.6 V *vs.* SHE to produce formic acid, while theoretical water electrolysis potential is +1.23 V *vs.* SHE. The fabricated PEM CO_2 conversion cell mimics a conventional PEM fuel cell, which works in the reverse principle of them. Hence, the required potential to split water at anode and transfer protons and electrons to cathode in the present case is expected to be higher than +1.23 V *vs.* SHE. Here, the cell potential is caused by the possible overpotentials only, which may arise from several factors, including resistance, diffusion and concentration.[38] Hence, we optimised the applied cell potential by determining conversion rates at various potential in discontinuous flow mode, while all other parameters are unchanged (Fig. 9). The conversion rate at various cell potential in discontinuous flow mode is presented in Fig. 10, which shows that the formic acid formation rate is maximum at +2.1 V w.r.t. cathode (*i.e.* +1.5 V *vs.* SHE). We observed no significant change in efficiency at higher potentials. Hence, +1.5 V potential was potentiostatically applied to anode w.r.t. cathode, in such a way that the total cell potential become +2.1 V. Pt/MWNTs–PIL also shows nearly similar trend with potential except the higher conversion rate.

In a typical CO_2 conversion experiment, the cell was activated by increasing the cell potential from 1.9 to 2.2 V by 0.1 V step, with a 15 min step-width, where both reservoirs were filled with DI water. This is analogous to the activation step in fuel cell. In all experiments, 2.1 V positive potential was applied to the cell continuously to the anode side of the cell with respect to

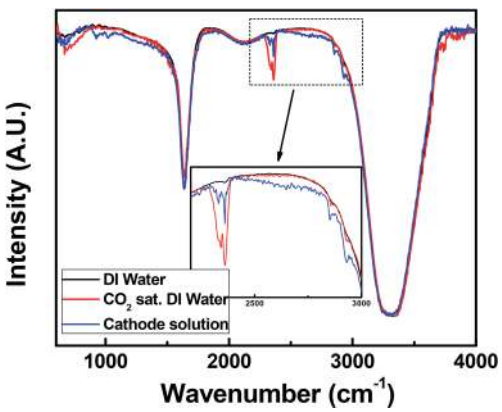

Fig. 7 FTIR spectrum of pure DI water, CO_2 saturated DI water and cathode reservoir solution (after 90 min of reaction).

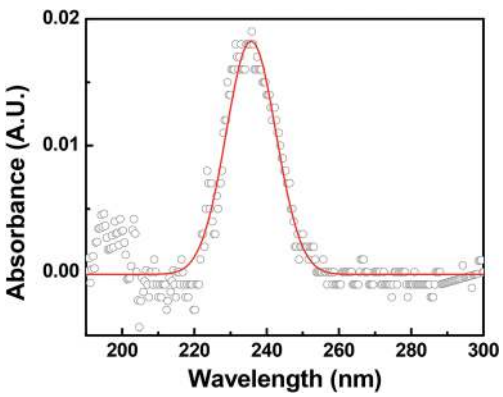

Fig. 8 Typical optical absorption spectra of cathode reservoir solution (recorded with Pt/MWNTs cathode in DF mode after 90 min reaction).

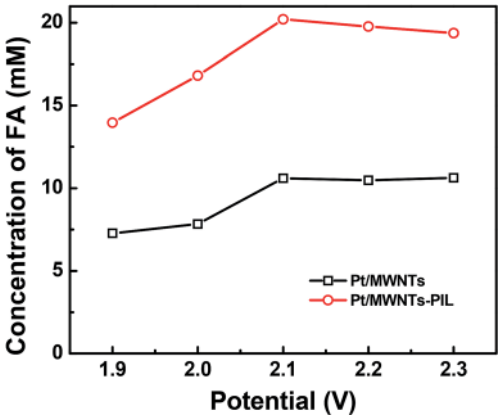

Fig. 9 Determination of working potential of PEM CO_2 conversion cell by discontinuous flow mode with 60 min conversion time per each data.

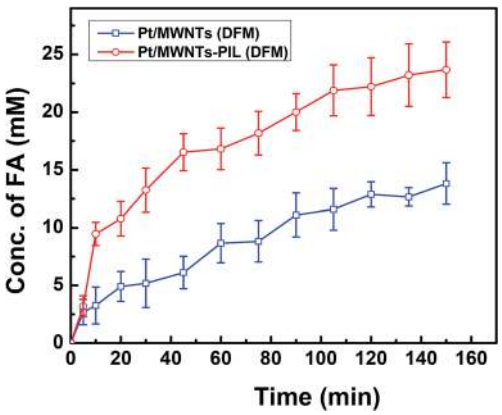

Fig. 10 Electrochemical formic acid (FA) formation from CO_2 on Pt/MWNTs and Pt/MWNTs–PIL cathode PEM cell in discontinuous flow (DF) mode.

cathode in order to split water into protons, electrons and gaseous oxygen at anode as given in eqn (1).

$$2H_2O \rightarrow 4H^+ + 4e^- + O_2 \quad (1)$$

The produced protons were transferred to cathode side of the cell through the Nafion membrane. Protons and electrons react with dissolved CO_2 molecules on the surface of catalyst and produce formic acid, which is a competing reaction of hydrogen production. In order to limit the product distribution, the cell was powered in potentiostatic mode.

$$H^+ + e^- \rightarrow H_{ad} \quad (2a)$$

$$CO_2 + H_{ad} \rightarrow HCOO_{ad} \quad (2b)$$

$$HCOO_{ad} + H_{ad} \rightarrow HCOOH \quad (2c)$$

$$H_{ad} + H_{ad} \rightarrow H_2 \quad (2d)$$

We believe that electroreduction of CO_2 into formic acid is a three step process as given in eqn (2).[22,37] In the first step (eqn (2a)), a proton is adsorbed on the surface of Pt catalyst along with an electron and forms adsorbed hydrogen atom (H_{ad}). In the second step (eqn (2b)), CO_2 molecules interact with the adsorbed hydrogen (H_{ad}) at the three-phase boundary and form an adsorbed formate radical ($HCOO_{ad}$). In the third step (eqn (2c)), adsorbed formate radical takes another H_{ad} to produce formic acid molecules and is desorbed from the conversion site.[37] Conclusively, 2 protons and 2 electrons convert a CO_2 molecule to formic acid. Nevertheless, production of H_2 molecule from recombination of two H_{ad} is also a possible competing reaction, which is similar to the reverse action of hydrogen – spill – over on catalyst surfaces. Finally, dissolved formic acid in deionised water at cathode reservoir was sampled at certain time interval and analysed by spectrophotometric techniques.[5]

Discontinues flow (DF) mode. In DF mode, cathode reservoir was filled with 40 ml of CO_2 saturated DI water and continuously circulated, while anode reservoir holds DI water, *i.e.*, CO_2 supply was stopped after saturation in DF mode (ESI 3†). The concentration of formic acid in the cathode reservoir solution of Pt/MWNTs and Pt/MWNTs–PIL cathode electrocatalyst based cells has been determined at certain time intervals up to 150 min of reaction time. Fig. S2 and S3† are the typical set of optical absorption spectra of cathode reservoir solution of Pt/MWNTs and Pt/MWNTs–PIL based CO_2 conversion cell in DF mode. The intensity increases with reaction time suggesting continues conversion of CO_2 into formic acid. The obtained spectra were fitted to Gaussian function after baseline correction and the peak height of the function was taken as peak intensity to calculate HCOOH concentration in cathode reservoir solution.

The final product of cathode reservoir shows the formic acid concentration as 24 ± 2 mM for Pt/MWNTs–PIL cathode, while it is 14 ± 2 mM for Pt/MWNTs after 150 min reaction in discontinuous flow mode (Fig. 10). Fig. 10 clearly suggests that the PIL functionalization increases the hydrocarbon production, which can be attributed to the good affinity of cathode material towards CO_2 molecules. A similar improvement has been observed in literature in CO_2 reduction in IL medium at lower overpotential.[17,35] In addition, the reduced particle size of Pt nanoparticles on MWNTs–PIL support significantly increases the physical and electrochemical surface area, which significantly increases the rate of reaction. The curves tent to saturate due to the continuously decreasing CO_2 concentration in the cathode solution.

Continues flow (CF) mode. In the CF mode, high pure CO_2 gas was continuously supplied (20 sccm) to the cathode reservoir solution throughout the experiment and the formic acid concentration was monitored continuously using a spectrophotometer (Fig. S4 and S5†). The analysis of cathode reservoir solution shows that Pt/MWNTs–PIL cathode produces 41 ± 6 mM formic acid from CO_2 saturated deionised water with 150 min reaction in CF mode, while it is 29 ± 4 mM for Pt/MWNTs cathode material (Fig. 11). Once again, the advantage of PIL functionalization has been demonstrated. The significant improvement in comparison with DF mode can be attributed to the retention of available CO_2 concentration by continuous

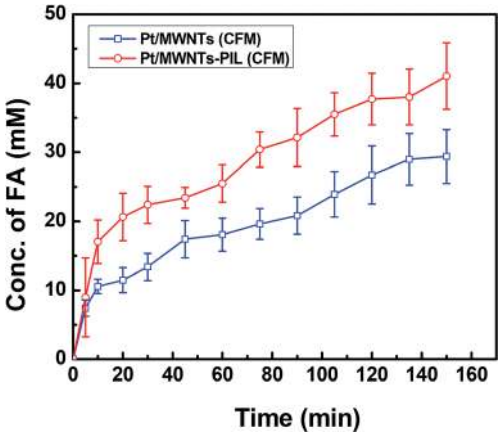

Fig. 11 Electrochemical formic acid (FA) formation from CO_2 on Pt/MWNTs and Pt/MWNTs–PIL cathode PEM cell in continuous flow (CF) mode.

flow. It is worth to note that the curves in CFM are straight, which suggests that the conversion rate is consistent till the reactants are supplied.

Mechanism. The enhancement in formic acid formation rate upon PIL functionalization has to be imputed to the efficient utilization of produced protons. Aeshala *et al.*, have reported 50% less loss of protons from H_2 generation upon introduction of CO_2 anchoring functional groups in the solid polymer electrolyte.[23] Since H_2 generation and CO_2 protonation are the mutually competing reactions, the favourability of reaction has been decided by local surface chemistry. In the present case, PIL functionalization accumulates CO_2 molecules at the three phase boundary. Furthermore, Pt active catalyst prevents H_2 generation when other competing reactions are possible. This effectively increases the localized concentration of reactants (H^+, e^- and CO_2) around active catalyst sites (Fig. 12). The higher local reactant concentration facilitates formic acid formation according to rate law of chemical reactions, since reaction rate is proportional to the concentration of reactants. In addition, it is observed that the particle size of Pt has been reduced much significantly on MWNTs–PIL, which also has to be imputed to the enhanced formic acid formation.

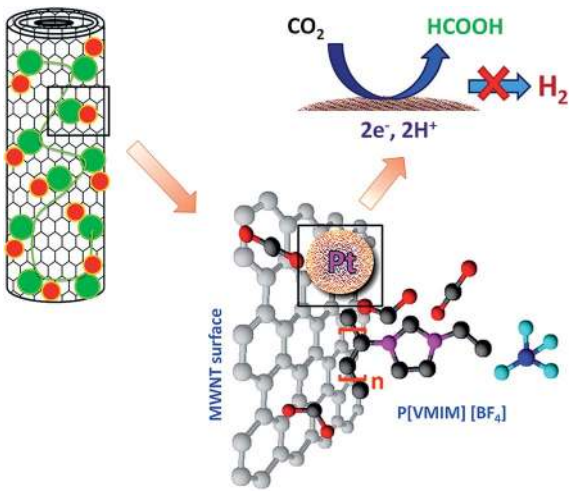

Fig. 12 Schematic representation of the mechanism behind the enhancement in performance.

These PIL functionalized catalyst supports will be promising in CO_2 conversion devices due to their good selectivity towards CO_2, where such devices can directly capture CO_2 from atmosphere and convert to fuels at ambient conditions. Furthermore, these devices will allow us to tune the experimental conditions and active catalyst to obtain selective hydrocarbon product with high efficiency.

4. Conclusion

In this report, we have shown that polymerized ionic liquid functionalized carbon nanotubes, when employed as a cathode catalyst support material in PEM based electrochemical cell, converts effectively CO_2 into formic acid. This novel support material with a high electrochemical surface area shows extremely good affinity towards CO_2. Besides, PIL functionalized MWNTs anchors the Pt nanoparticles better than MWNTs and produce good dispersion of fine particles. The electrochemical CO_2 conversion on synthesized catalysts has been studied in discontinuous and continuous flow mode, which shows a significant improvement in conversion rate upon PIL functionalization. The improvement has been attributed to the good affinity and weak intermediate formation of catalyst support with CO_2 and smaller particle size. Continuous flow of CO_2 gas increases the formic acid production rate, suggesting the ability of the device in continuous operation. Thus, the developed device effectively combines CO_2 with a water molecule (*i.e.*, 2 protons and 2 electrons) and produces formic acid.

Acknowledgements

Authors acknowledge SAIF-IITM for FTIR analysis. One of the authors (Tamilarasan P.) acknowledges Indian Institute of Technology Madras (IITM) for the financial supports (senior research fellowship).

References

1 E. V. Kondratenko, G. Mul, J. Baltrusaitis, G. O. Larrazabal and J. Perez-Ramirez, *Energy Environ. Sci.*, 2013, **6**, 3112–3135.
2 S. Das and W. M. A. Wan Daud, *RSC Adv.*, 2014, **4**, 20856–20893.
3 Q. Wang, H. Dong, H. Yu, H. Yu and M. Liu, *RSC Adv.*, 2015, **5**, 10346–10351.
4 C. Ampelli, G. Centi, R. Passalacqua and S. Perathoner, *Energy Environ. Sci.*, 2010, **3**, 292–301.
5 S. R. Narayanan, B. Haines, J. Soler and T. I. Valdez, *J. Electrochem. Soc.*, 2011, **158**, A167–A173.
6 C. Delacourt, P. L. Ridgway, J. B. Kerr and J. Newman, *J. Electrochem. Soc.*, 2008, **155**, B42–B49.
7 M. Alvarez-Guerra, S. Quintanilla and A. Irabien, *Chem. Eng. J.*, 2012, **207–208**, 278–284.

8 M. Alvarez-Guerra, A. Del Castillo and A. Irabien, *Chem. Eng. Res. Des.*, 2014, **92**, 692–701.
9 W. Yuan, S. Lu, Y. Xiang and S. P. Jiang, *RSC Adv.*, 2014, **4**, 46265–46284.
10 J. B. Xu and T. S. Zhao, *RSC Adv.*, 2013, **3**, 16–24.
11 P. C. Sherrell, W. Zhang, J. Zhao, G. G. Wallace, J. Chen and A. I. Minett, *ChemSusChem*, 2012, **5**, 1233–1240.
12 V. Mittal, *Surface Modification of Nanotube Fillers*, 2011, pp. 1–23.
13 S. H. Shuit, K. F. Yee, K. T. Lee, B. Subhash and S. H. Tan, *RSC Adv.*, 2013, **3**, 9070–9094.
14 H. Li, P. S. Bhadury, B. Song and S. Yang, *RSC Adv.*, 2012, **2**, 12525–12551.
15 T. Nonthanasin, A. Henni and C. Saiwan, *RSC Adv.*, 2014, **4**, 7566–7578.
16 Z.-Z. Yang, Y.-N. Zhao and L.-N. He, *RSC Adv.*, 2011, **1**, 545–567.
17 B. A. Rosen, J. L. Haan, P. Mukherjee, B. Braunschweig, W. Zhu, A. Salehi-Khojin, D. D. Dlott and R. I. Masel, *J. Phys. Chem. C*, 2012, **116**, 15307–15312.
18 S. Supasitmongkol and P. Styring, *Energy Environ. Sci.*, 2010, **3**, 1961–1972.
19 B. J. Adzima, S. R. Venna, S. S. Klara, H. He, M. Zhong, D. R. Luebke, M. S. Mauter, K. Matyjaszewski and H. B. Nulwala, *J. Mater. Chem. A*, 2014, **2**, 7967–7972.
20 P. Tamilarasan, T. Remya and S. Ramaprabhu, *Graphene*, 2013, **1**, 3–10.
21 P. Tamilarasan and S. Ramaprabhu, *J. Mater. Chem. A*, 2015, **3**, 101–108.
22 P. Tamilarasan and S. Ramaprabhu, *J. Mater. Chem. A*, 2015, **3**, 797–804.
23 L. M. Aeshala, R. Uppaluri and A. Verma, *Phys. Chem. Chem. Phys.*, 2014, **16**, 17588–17594.
24 B. P. Sullivan, *Platinum Met. Rev.*, 1989, **33**, 2–9.
25 Q. Luo, G. Feng, M. Beller and H. Jiao, *J. Phys. Chem. C*, 2012, **116**, 4149–4156.
26 M. M. Shaijumon and S. Ramaprabhu, *Chem. Phys. Lett.*, 2003, **374**, 513–520.
27 B. Wu, D. Hu, Y. Kuang, B. Liu, X. Zhang and J. Chen, *Angew. Chem., Int. Ed.*, 2009, **48**, 4751–4754.
28 B. Wu, D. Hu, Y. Kuang, B. Liu, X. Zhang and J. Chen, *Angew. Chem., Int. Ed.*, 2009, **48**, 4751–4754.
29 N. B. Colthup, L. H. Daly and S. E. Wiberley, *Introduction to infrared and Raman spectroscopy*, Elsevier, 1990.
30 N. B. Colthup, *J. Opt. Soc. Am.*, 1950, **40**, 397–400.
31 P. Tamilarasan and S. Ramaprabhu, *J. Mater. Chem. A*, 2015, **3**, 101–108.
32 Y. Hori, in *Modern Aspects of Electrochemistry*, ed. C. Vayenas, R. White and M. Gamboa-Aldeco, Springer, New York, 2008, vol. 42, pp. 89–189.
33 G. Lu, H. Wang, Z. Bian and X. Liu, *Sci. World J.*, 2013, **2013**, 8.
34 J. L. Haan, *Electrochemistry of Formic Acid and Carbon Dioxide on Metal Electrodes with Applications to Fuel Cells and Carbon Dioxide Conversion Devices*, University of Illinois at Urbana-Champaign, 2010.
35 D. C. Grills, Y. Matsubara, Y. Kuwahara, S. R. Golisz, D. A. Kurtz and B. A. Mello, *J. Phys. Chem. Lett.*, 2014, **5**, 2033–2038.
36 M. Łukaszewski, H. Siwek and A. Czerwiński, *J. Solid State Electrochem.*, 2009, **13**, 813–827.
37 Y. B. Vassiliev, V. S. Bagotzky, O. A. Khazova and N. A. Mayorova, *J. Electroanal. Chem. Interfacial Electrochem.*, 1985, **189**, 295–309.
38 O. E. Herrera, D. P. Wilkinson and W. Mérida, *J. Power Sources*, 2012, **198**, 132–142.